



Finite Element Simulation of Mixed-Mode PV Encapsulant Delamination Based on Cohesive Zone Model

Preprint

Xin He and Nick Bosco
National Renewable Energy Laboratory

*Presented at the at the 2018 World Conference on Photovoltaic Energy Conversion (WCPEC-7)
Waikoloa, Hawaii
June 10–15, 2018*

© 2018 IEEE. Personal use of this material is permitted. Permission from IEEE must be obtained for all other uses, in any current or future media, including reprinting/republishing this material for advertising or promotional purposes, creating new collective works, for resale or redistribution to servers or lists, or reuse of any copyrighted component of this work in other works.

Suggested Citation

He, Xin, and Nick Bosco. 2018. "Finite Element Simulation of Mixed-Mode PV Encapsulant Delamination Based on Cohesive Zone Model: Preprint." Golden, CO: National Renewable Energy Laboratory. NREL/CP-2C00-71725. <https://www.nrel.gov/docs/fy19osti/71725.pdf>.

**NREL is a national laboratory of the U.S. Department of Energy
Office of Energy Efficiency & Renewable Energy
Operated by the Alliance for Sustainable Energy, LLC**

This report is available at no cost from the National Renewable Energy Laboratory (NREL) at www.nrel.gov/publications.

Conference Paper
NREL/CP-2C00-71725
October 2018

Contract No. DE-AC36-08GO28308

NOTICE

This work was authored by the National Renewable Energy Laboratory, operated by Alliance for Sustainable Energy, LLC, for the U.S. Department of Energy (DOE) under Contract No. DE-AC36-08GO28308. Funding provided as part of the Durable Modules Consortium (DuraMAT), an Energy Materials Network Consortium, funded by the U.S. Department of Energy, Office of Energy Efficiency & Renewable Energy, Solar Energy Technologies Office. The views expressed in the article do not necessarily represent the views of the DOE or the U.S. Government. The U.S. Government retains and the publisher, by accepting the article for publication, acknowledges that the U.S. Government retains a nonexclusive, paid-up, irrevocable, worldwide license to publish or reproduce the published form of this work, or allow others to do so, for U.S. Government purposes.

This report is available at no cost from the National Renewable Energy Laboratory (NREL) at www.nrel.gov/publications.

U.S. Department of Energy (DOE) reports produced after 1991 and a growing number of pre-1991 documents are available free via www.OSTI.gov.

Cover Photos by Dennis Schroeder: (left to right) NREL 26173, NREL 18302, NREL 19758, NREL 29642, NREL 19795.

NREL prints on paper that contains recycled content.

Finite Element Simulation of Mixed-Mode PV Encapsulant Delamination Based on Cohesive Zone Model

Xin He and Nick Bosco

National Renewable Energy Laboratory, Golden, CO, 80403, US

Abstract—A finite element model (FEM) was developed to simulate the mixed-mode delamination failure at the encapsulant’s interface within PV modules under mixed-mode loading conditions. Parameters to characterize the bilinear traction-separation constitutive behavior of cohesive elements were determined by testing the pure mode I critical fracture energy of the photovoltaic (PV) cell interface using the width-tapered beam and fitting the simulated load-displacement curve with the measured curve. This developed FEM can be used to predict the critical temperature changes, at which delamination would initiate, for PV modules with different sizes and provide guidance for the design of PV module with better reliability.

Index Terms—Finite element model (FEM), Cohesive zone model (CZM), Photovoltaic cells, Mixed-mode delamination, Delamination fracture energy.

I. INTRODUCTION

Within a photovoltaic (PV) module, there exists a complex, and varying, loading condition at the encapsulant’s interfaces that serves as the driving force for delamination. In fracture mechanics, these loading conditions are defined as one, or a combination of three modes, mode I: opening, mode II: in-plane shear, and mode III: out of plane shear. While recent efforts have been focused on developing the metrology to and assessing the mode I critical fracture energy of the PV module encapsulant’s interface [1]-[3], characterization of the mode II and III fracture behavior is absent. Furthermore, knowledge of the mixed-mode driving force at the PV module’s encapsulant interfaces is not well understood. In order to predict and simulate when and how delamination failure occurs in a PV module, both these details of driving force and fracture condition must be characterized.

For mode II, III or mixed-mode loading, the shear stress at the encapsulant’s interface is the relevant stress tensor. With the application of a thermomechanical strain, this shear stress will increase from the center of each cell with the maximum being reached at its outer corner, suggesting delamination would initiate at the outer corner of a cell and propagate towards its center. Due to a stress singularity caused by the high stress concentration at the cell’s sharp corner and the complexity of the three-dimensional (3-D) stress analysis, the exact stress field is difficult to be describe accurately by any theoretical model. Therefore, a finite element model (FEM) is an excellent tool to conduct the stress analysis and simulate the delamination failure in a PV module. Currently, the most widely used model to simulate fracture is the cohesive zone model (CZM) with the bilinear traction-separation constitutive law [4]-[5]. By inserting cohesive elements at the

encapsulant’s interfaces and assigning appropriate parameters to characterize the constitutive law, the mixed-mode delamination fracture behavior of the encapsulant’s interfaces in PV modules can be accurately predicted.

The bilinear traction-separation law, as shown in Fig. 1, is controlled by three parameters along each direction, the initial stiffness (K_I, K_{II}, K_{III}), the strength (T_I, T_{II}, T_{III}), and the critical fracture energy ($G_{Ic}, G_{IIc}, G_{IIIc}$), the subscripts I, II , and III denote the three loading conditions. The initial stiffness should be high enough to avoid any effect on the overall compliance and small enough to avoid spurious oscillations in the tractions [5]. In this constitutive law, the stress in the cohesive element will increase proportionally to the increase of separation until the strength, T , is reached. At this point, fracture will initiate and the corresponding separation is denoted as Δ^c . With further loading, the stress in the cohesive element will be released and the cohesive element will be eliminated once the critical fracture energy, G_c , is reached (the separation is Δ^{fail} at this point). Δ^c and Δ^{fail} can be calculated based on T , K , and G_c using equations (1) and (2).

$$\Delta^c = \frac{T}{K} \quad (1)$$

$$\Delta^{final} = \frac{2G_c}{T} \quad (2)$$

For a uniform interface, $G_{IIc} = G_{IIIc}$, $K_{II} = K_{III}$, and $T_{II} = T_{III}$, therefore, only G_{Ic} , G_{IIc} , K_I , K_{II} , T_I , and T_{II} need to be determined.

In this study, preliminary experiments were first conducted to determine the bilinear traction-separation law parameters for two PV laminate systems. Then a FEM of a PV module laminate with the characterized CZM at the encapsulant/Si PV cell interface was constructed to simulate and predict the mixed-mode delamination fracture behavior under different thermal loading conditions.

II. PRELIMINARY EXPERIMENTS AND MODELING

A. Width-tapered cantilever beam test to determine G_{Ic}

Two ethylene vinyl acetate (EVA)/Si PV cell interfaces were chosen to be measured and simulated in this study. One with a known high critical fracture energy (high G_c), and one with a known low critical fracture energy (low G_c). The bulk properties of the materials are otherwise the same. The choice to include a low G_c interface was made to help

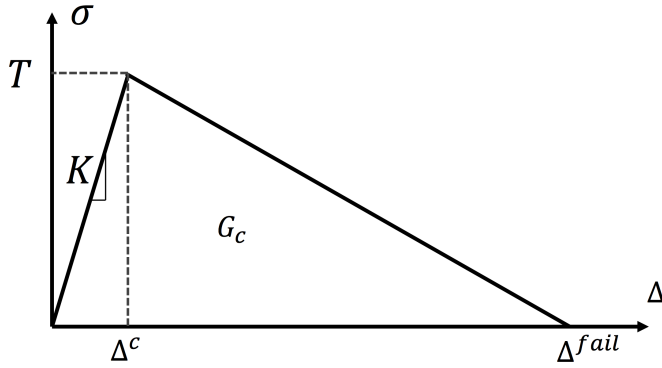


Fig. 1. Bilinear traction-separation law of cohesive elements [6].

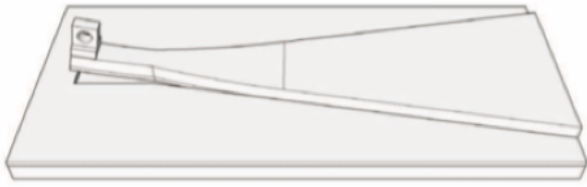


Fig. 2. Cartoon of a width-tapered single cantilever beam sample. The sample is loaded via the tap placed at the apex of its beam [3].

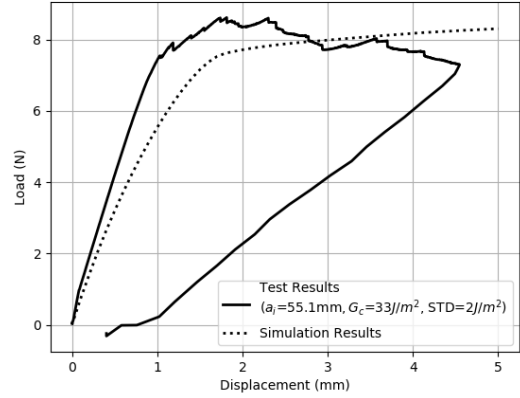
illustrate the delamination process in the subsequent module-level simulations. Samples were fabricated by laminating a crystalline Si PV cell to a slide of glass with each EVA.

Aimed to obtain the mode I critical delamination fracture energy, G_{Ic} , the width-tapered cantilever beam test developed by Bosco [3] was conducted on the low and high G_c interfaces. The general idea of this testing method is to adhere the elastic width-tapered cantilever beam to the cell surface, Fig. 2. When the beam is loaded at its apex, delamination will initiate and advance upon continued loading. For the low G_c material, a titanium width-tapered beam with a thickness of 0.86mm was used while a thicker titanium beam (thickness: 1.6mm) was used for the high G_c material. The detailed testing procedures can be found in [3].

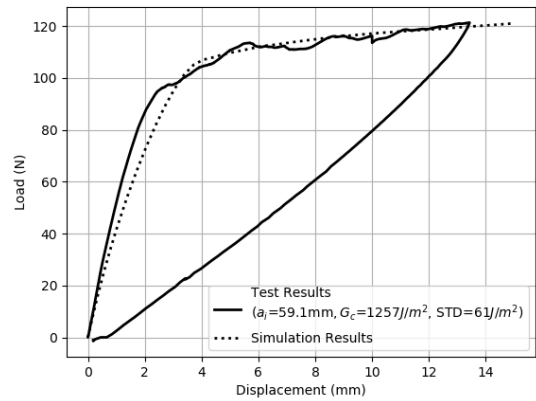
Based on the measured crack length (a_i), plateau load (P_c) and the final load-line displacement (Δ_i), G_{Ic} can be calculated using equation (3), where θ is the apex angle of the width-tapered beam and equal to 20° in this study.

$$G_{Ic} = \frac{P_c \Delta_i}{2a_i^2 \tan(\theta/2)} \quad (3)$$

The tested load-displacement curves for both interfaces are shown in Fig. 3. As shown in Fig. 3(a), the final crack length of the low G_c material is 55.1mm and the calculated G_{Ic} is $33\text{J}/\text{m}^2$ with a standard deviation (STD) of $2\text{J}/\text{m}^2$. Similarly, Fig. 3(b) indicates the final crack length is 59.1mm



(a)



(b)

Fig. 3. Tested and simulated load-displacement curves for: (a) low G_c material; and (b) high G_c material.

for the high G_c material and G_{Ic} is $1257\text{J}/\text{m}^2$ with a STD of $61\text{J}/\text{m}^2$.

B. Modeling to determine K_I and T_I

In order to determine the initial stiffness K_I and the strength T_I , a FEM based on CZM was developed using the commercial software ABAQUS 6.13 to simulate the width-tapered cantilever beam test as shown in Fig. 4. In this model a thin layer of cohesive elements, highlighted as the red trapezoid were inserted at the cell/EVA interface and a velocity boundary condition ($1\text{mm}/\text{s}$) was applied at the loading hole to displace the beam and enable the delamination process. Initially, all layers are combined.

The thicknesses and material properties used in this simulation are summarized in Table 1 where the Young's modulus of the titanium beam was obtained by fitting the unloading compliance while the thickness and material properties for cell and EVA were generated from [9].

K_I and T_I for the cohesive elements were found by fitting the simulated load-displacement curves to the experimental

TABLE 1

SUMMARY OF THICKNESS AND MATERIAL PROPERTIES FOR EACH LAYER IN FEM [9].

Layers	Thickness(mm)	Young's modulus(GPa)	Poisson ratio
Beam	0.86 for structure I, 1.6 for structure II	69.5	0.342
Cell	0.175	170	0.28
EVA	0.45	0.01442	0.4995
Cohesive layer	0.002	none	none

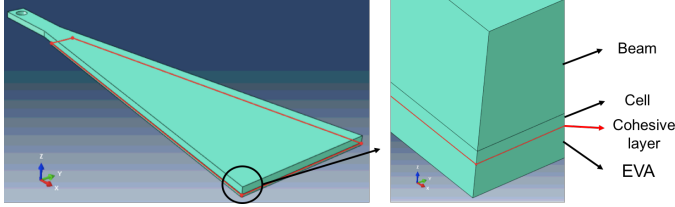


Fig. 4. FEM to simulate the width-tapered cantilever beam test.

result. The simulated load-displacement curves for both structures and the comparison with the testing results are shown in Fig. 3.

As shown in Fig. 3(a), a good match was obtained between the simulated and measured load-displacement curves for the low G_c material by choosing T_I as $0.2MPa$ and K_I as $100MPa/mm$. For the high G_c material, simulation with $K_I = 100MPa/mm$ and $T_I = 4MPa$ yielded a load-displacement curve that is in excellent agreement with the experimental result as shown in Fig. 3(b).

Note that in addition, both Fig. 3(a) and 3(b) show a lower simulated stiffness at the initial loading stage. This is caused by the damage mechanism of the cohesive elements. Refer to the bilinear traction-separation behavior shown in Fig. 1, the stress in the cohesive elements will be released once the strength is reached which acts to lower the stiffness of the overall structure.

C. Determination of G_{IIc} , K_{II} , and T_{II}

Recall that the initial stiffness is a penalty parameter and we have shown $K_I = 100MPa/mm$ is high enough and will not affect the overall stiffness, therefore, $K_{II} = K_{III} = 100MPa/mm$ should also be high enough to avoid the effect of cohesive element on the shear stiffness of the overall structure as $G = \frac{E}{2(1+\nu)} < E$, where G is the shear modulus, E is the Young's modulus and ν is the Poisson ratio. Based on this fact, $K_{II} = K_{III} = 100MPa/mm$ was applied in this study.

Typically, the mode II critical fracture energy, G_{IIc} , is 3 to 5 times of the mode I critical fracture energy, G_{Ic} . Also the strength, T_{II} is proportional to G_{IIc} according to equation (2). In order to maximum the mode mixity, a smaller T_{II} should be used to enable the mode II and mode III delamination occur earlier and yield a higher G_{IIc} and G_{IIIc} . Hence, we assumed $G_{IIc} = 3G_{Ic}$ and $T_{II} = 3T_I$.

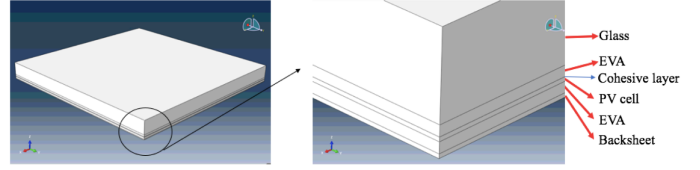


Fig. 5. FEM to simulate the mixed-mode delamination at cell/EVA interface in a PV module with one cell.

III. MIXED-MODE DELAMINATION SIMULATION OF PV ENCAPSULANT UNDER TEMPERATURE CHANGE

The purpose of this study is to investigate the mixed-mode delamination of the cell/EVA interface in the PV module through temperature change. The parameters of the low G_c material are applied as a higher critical fracture energy would prevent delamination under the simulated conditions. The other parameters to characterize the CZM are summarized following:

$$K_I = K_{II} = K_{III} = 100MPa/mm \quad (4)$$

$$T_I = 0.2MPa \quad (5)$$

$$G_{IIc} = G_{IIIc} = 3G_{Ic} = 99J/m^2 \quad (6)$$

$$T_{II} = T_{III} = 2T_I = 0.6MPa \quad (7)$$

A one cell PV module laminate (size $100mm \times 100mm$) was studied. The FEM is shown in Fig. 5, in which a thin cohesive elements were applied at the cell and front EVA interface. In this model, symmetric boundary conditions were applied at both rear left and right side faces (quarter model), and the bottom corner of backsheet layer located at the origin was fixed. The material properties and geometry constants used in this model are summarized in Table 2. The Young's modulus and thermal expansion coefficient (TEC) of EVA is a function of temperature (T) according to [9]. Similarly to the FEM model of width-tapered cantilever beam test, the backsheet and cell were simulated using C3D8 elements, while the EVA layer was simulated using C3D8H elements and COH3D8 elements were used to simulate the cohesive layer.

TABLE 2

SUMMARY OF THICKNESS AND MATERIAL PROPERTIES FOR EACH LAYER IN FEM [9].

Layers	Thickness(mm)	Young's modulus(GPa)	Poisson ratio	TEC ($10^{-6}/K$)
Backsheet	0.175	3.2	0.4	150
Cell	0.175	170	0.28	2.6
EVA	0.45	$(522.391 - 2.92693T + 0.00410263T^2)/1000$	0.4995	$0.02487 + 0.0001508T - 6.51e - 6T^2 + 4.728e - 8T^3 - 1.362e - 10T^4 + 1.41e - 13T^5$
Cohesive layer	0.002	none	none	none

A. Mixed-mode delamination under temperature change $145^\circ C$ to $-40^\circ C$

In this simulation an initial temperature field of $145^\circ C$ was applied (zero stress state at $145^\circ C$), then the temperature was reduced to $-40^\circ C$ in 46 seconds.

The results of this simulation show fracture energy is initially developed (about 1% of G_{Ic}) at the outer corner (top right) of the cell at $55^\circ C$ (temperature change $-90^\circ C$). The distribution of fracture energy in the cohesive layer at this temperature is shown in Fig. 6(a). When the structure was cooled further to $17.8^\circ C$ (temperature change: $-127.2^\circ C$), the cohesive elements at the outer corner are eliminated as they achieve the critical fracture condition and the delamination propagates toward the center of the cell as shown in Fig. 6(b). Directly preceding delamination, the total fracture energy at this location is $35.9 J/m^2$. Based on the mixed-mode fracture criterion (Equation (8)) and the expression of total fracture energy (Equation (9)), we can solve $G_I = 31.55 J/m^2$, $G_{II} = G_{III} = 2.175 J/m^2$. Using the solved fracture energy components, the mode mixity can be obtained as $m_1 = G_I/35.9 = 0.879$, $m_2 = m_3 = G_{II}/35.9 = 0.0545$, which indicate this delamination was mainly caused by a mode I driving force.

$$\frac{G_I}{G_{Ic}} + \frac{G_{II}}{G_{IIc}} + \frac{G_{III}}{G_{IIIc}} = \frac{G_I}{33} + 2\frac{G_{II}}{99} = 1 \quad (8)$$

$$G_I + G_{II} + G_{III} = 35.9 J/m^2 \quad (9)$$

At a temperature change of $-141.6^\circ C$, the delamination pattern, which is the pattern of the eliminated cohesive elements, is presented in Fig. 7.

B. Mixed-mode delamination under temperature change $25^\circ C$ to $-160^\circ C$

In this simulation, the structure was cooled from $25^\circ C$ to $-160^\circ C$ in 37 seconds (zero stress state at $25^\circ C$). Compared to the simulation in last section (zero stress state at $145^\circ C$), the driving force for delamination in this simulation is altered by considering a lower temperature regime and the temperature dependent properties of EVA. In reality, PV modules may not undergo this wide temperature range during the service period.

This simulation demonstrates that fracture energy is initially developed (about 1% of G_{Ic}) at a temperature of $-5^\circ C$ (temperature change of $-30^\circ C$), again at the outer corner of the cell as shown in Fig. 8(a). This temperature change is considerably less than the temperature change ($-90^\circ C$) required

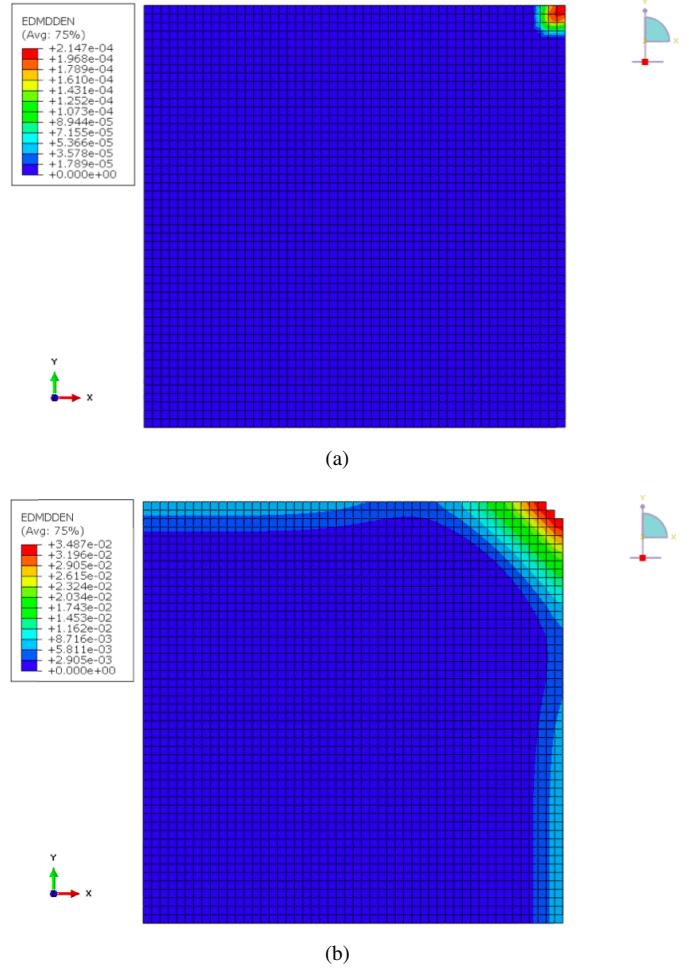


Fig. 6. Distribution of total fracture energy in the cohesive layer when: (a) delamination starts to initiate; and (b) delamination starts to propagate at the outer corner.

to develop the same fracture energy in the previous, higher absolute temperature, simulation. This difference manifests from operating in a lower temperature regime where the EVA is much stiffer, thereby more capable of transmitting stress through strain to develop fracture energy at the cell/EVA interface. Fig. 8(b) indicates that cohesive elements at the outer corner of the cell begin to be eliminated at a temperature of $-72.5^\circ C$ (temperature change $-97.5^\circ C$) in this simulation. This temperature change is again smaller than that required to initiate delamination in the previous simulation ($-127.2^\circ C$). Finally, a temperature change of $-120^\circ C$ develops a similar extent of delamination as the $-141.6^\circ C$ change when the

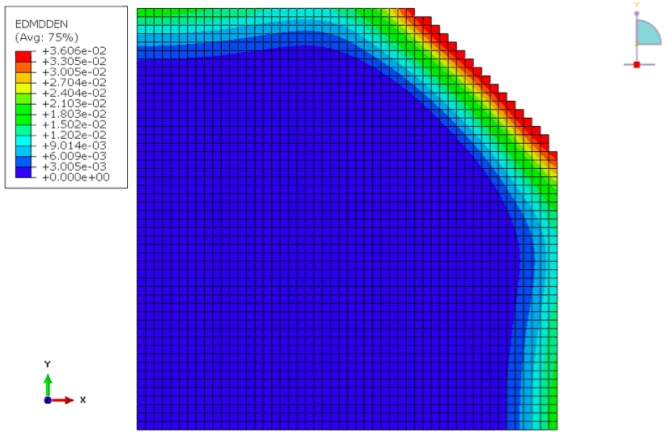


Fig. 7. Delamination pattern under temperature change from 145°C to 3.4°C .

zero stress state was at 145°C , Fig. 9. This result again demonstrates that a smaller temperature change is required to initiate and induce delamination when the encapsulant is stiffer.

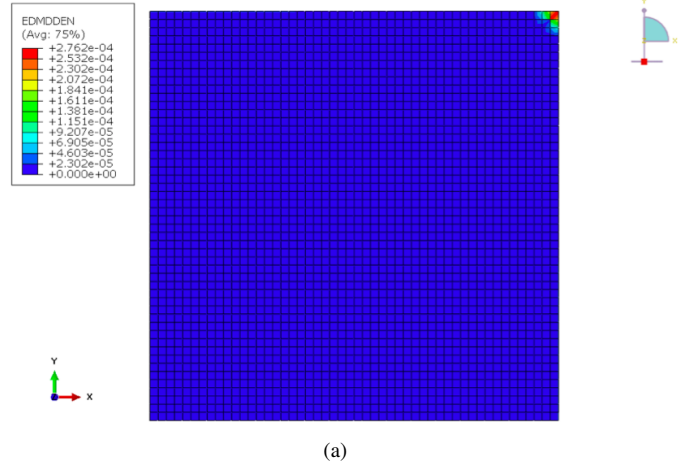
C. Mixed-mode delamination under temperature change 25°C to 80°C

In order to study the delamination behavior under heating, another simulation was run. In this simulation, the structure was heated from 25°C to 80°C in 27.5 seconds (zero stress state at 25°C) and no fracture energy was developed. Fig. 10, therefore, presents the distribution of out of plane stress along the thickness direction (σ_{zz}) in the cohesive layer. It indicates that this stress tensor is negative at the outer corner and the edges of the cell. Compressive mode I stress does not produce positive fracture energy. Therefore, when the PV module is heated, delamination at the cell/EVA interface may be dictated by the mode II and III driving forces.

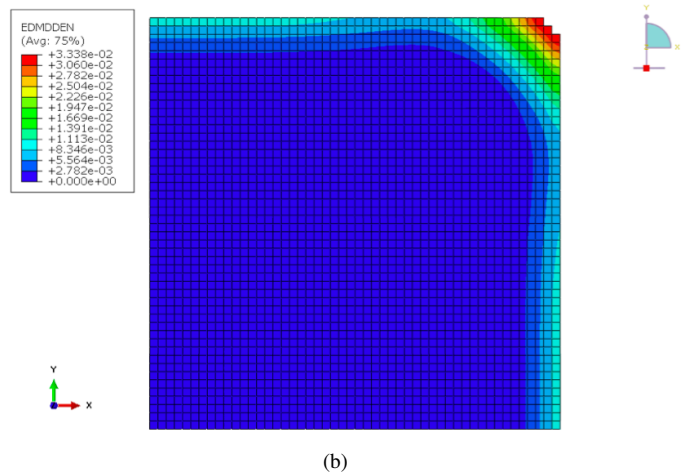
IV. SUMMARY AND CONCLUSIONS

In this study, a FEM based on CZM was developed to simulate the mixed-mode delamination at the EVA/Si PV cell interface in a one-cell PV module under thermal loading. The CZM was characterized by the bilinear traction-separation law and the parameters that control this constitutive law were generated through fitting the experimental results of a width-tapered cantilever beam test. By integrating the determined parameters to the FEM, the mixed-mode delamination behavior of the PV module was simulated under different temperature changes.

The results showed that delamination initiates at the outer corner of the EVA/Si PV cell interface when temperature is decreased from 145°C to 55°C , following which it propagates toward the center when the temperature decreased further. In addition, this delamination was mainly caused by a mode I driving force as the mode I mixity was calculated to be 87.9%. When a temperature change of 25°C to -160°C was prescribed, the temperature change required to develop



(a)



(b)

Fig. 8. Distribution of total fracture energy in the cohesive layer when: (a) delamination starts to initiate; and (b) delamination starts to propagate at the outer corner.

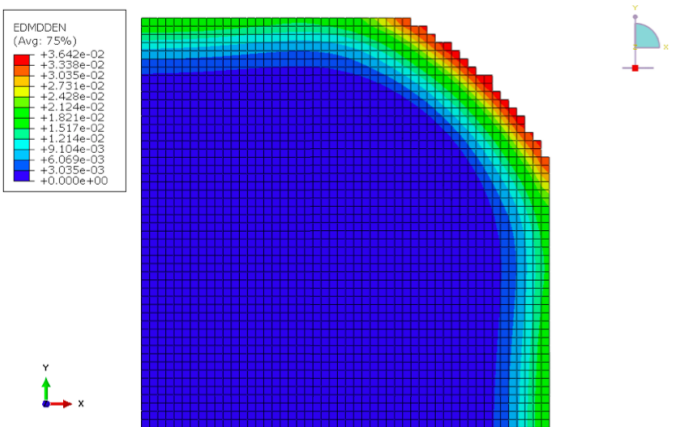


Fig. 9. Delamination pattern under temperature change from 25°C to -95°C .

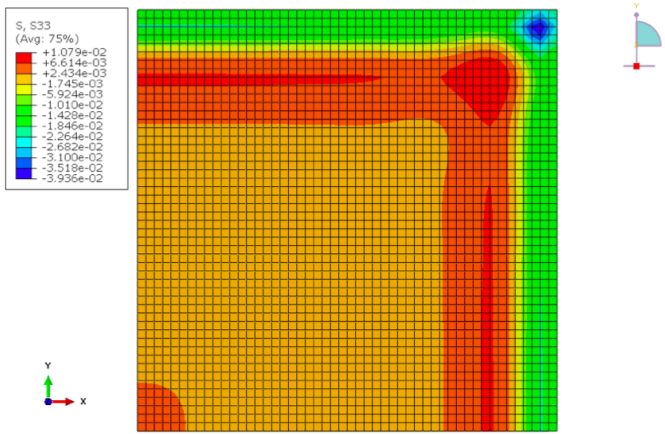


Fig. 10. Distribution of normal stress in cohesive layer under temperature change from 25°C to 80°C .

fracture energy and initiate the delamination is much less than that in the simulation with higher zero stress state temperature. This behavior manifests from the temperature dependent stiffness of the EVA: in the lower temperature regime EVA becomes stiffer and more capable of transmitting stress due to the CTE mismatch and temperature change. In contrast, delamination was not found to initiate under heating from 25°C to 80°C as the normal stress along the thickness direction, driving the mode I delamination, was negative. Therefore, within a heated PV module, the delamination at cell/EVA interface will be dictated by the mode II and III driving forces.

ACKNOWLEDGMENT

This work was supported by the U.S. Department of Energy (DOE) under Contract No. DE-AC36-08GO28308 with Alliance for Sustainable Energy, LLC, the Manager and Operator of the National Renewable Energy Laboratory (NREL). NREL is a national laboratory of the DOE, Office of Energy Efficiency and Renewable Energy. Funding provided as part of the Durable Modules Consortium (DuraMAT), an Energy Materials Network Consortium funded by the U.S. Department of Energy, Office of Energy Efficiency & Renewable Energy, Solar Energy Technologies Office.

REFERENCES

- [1] Shivakumar, R., Tippabhotla, S.K., Handara, V.A., Illya, G., Tay, A.A., Novoa, F., Dauskardt, R.H. and Budiman, A.S., "Fracture mechanics and testing of Interface adhesion strength in multilayered structures—application in advanced solar PV materials and technology", *Procedia Engineering* vol. 139, pp. 47-55, 2016.
- [2] Lin, C.C., Lyu, Y., Hunston, D.L., Kim, J.H., Wan, K.T., Stanley, D.L. and Gu, X., "Cracking and delamination behaviors of photovoltaic backsheets after accelerated laboratory weathering", *Reliability of Photovoltaic Cells, Modules, Components, and Systems VIII* vol. 9563, pp. 956304, 2015.

- [3] Bosco, N., Tracy, J., Dauskardt, R. and Kurtz, S., "Development and first results of the width-tapered beam method for adhesion testing of photovoltaic material systems", *In 43rd IEEE Photovoltaic Specialists Conference (PVSC)* vol. 9563, pp. 0106-0110, 2016.
- [4] Geubelle, P.H. and Baylor, J.S., "Impact-induced delamination of composites: a 2D simulation", *Composites Part B: Engineering* vol. 29, pp. 589-602, 1998.
- [5] Turon, A., Camanho, P.P., Costa, J. and Dvila, C.G., "A damage model for the simulation of delamination in advanced composites under variable-mode loading", *Mechanics of Materials* vol. 38, pp. 1072-1089, 2006.
- [6] Song, K., Dvila, C.G. and Rose, C.A., "Guidelines and parameter selection for the simulation of progressive delamination", *In ABAQUS Users Conference* vol. 41, pp. 43-44, 2008.
- [7] de Moura, M.F., "Interlaminar mode II fracture characterization", *In Delamination Behaviour of Composites*, pp. 310-326, 2008.
- [8] Davidson, B.D., "Standardization of the end-notched flexure test for Mode II interlaminar fracture toughness determination of unidirectional laminated composites", *Journal of Testing and Evaluation*, vol. 43, pp. 1540-1553, 2015.
- [9] Bosco, N., Silverman, T.J. and Kurtz, S., "Climate specific thermomechanical fatigue of flat plate photovoltaic module solder joints", *Microelectronics Reliability*, vol. 62, pp. 124-129, 2016.